9-15-1973

Raman Spectrum of Gadolinium Molybdate Above and Below the Ferroelectric Transition

Frank Ullman
University of Nebraska - Lincoln

B. J. Holden
University of Nebraska - Lincoln

B. N. Ganguly
Ganguly

John R. Hardy
University of Nebraska - Lincoln

Raman Spectrum of Gadolinium Molybdate above and below the Ferroelectric Transition*

Frank G. Ullman and B. J. Holden†‡
Electrical Materials Laboratory, Department of Electrical Engineering, University of Nebraska, Lincoln, Nebraska 68508

B. N. Ganguly and J. R. Hardy
Behlen Laboratory of Physics, University of Nebraska, Lincoln, Nebraska 68508

(Received 17 January 1973)

90°-scattered Raman spectra of single-domain gadolinium molybdate have been obtained at room temperature and above the 159 °C ferroelectric transition on several crystal orientations. Lines in the 0–200-cm^{-1} range can all be associated with Raman-active phonons and are identified by symmetry considerations, scattering-efficiency calculations, and comparison of spectra for different crystal orientations. Lines in the 200–1000-cm^{-1} range can be identified with coupled vibrations of tetrahedral molybdate ions. Spectra for frequencies above 1000 cm^{-1} originate from impurity flourescence. The effect of the presence of multiple domains on the spectra was determined; the observed differences between single-domain and multiple-domain crystals result from B_1-B_2 symmetry mixing from the twinning of adjacent domains. No new soft modes, in addition to the known soft mode at about 43 cm^{-1}, were observed. A few of the lines that are present in only the low-temperature phase cannot be identified from symmetry analysis and are probably derived from zone-boundary modes of the high-temperature phase.

I. INTRODUCTION

Gadolinium molybdate (GMO) is a new type of displacive ferroelectric in which the transition to the ferroelectric phase was first suggested to be triggered by an elastic-mode rather than an optic-mode instability.[1] To determine if any softening of optic modes or other unusual temperature-dependent properties were involved in the transition, an investigation of the Raman spectrum and its changes on heating from room temperature through the 159 °C ferroelectric transition T_c was undertaken. (The effect of the transition on several physical properties of GMO is discussed by Cummins.[2]) Not much has yet been reported on Raman scattering from GMO. Fleury[3] reported an apparent soft mode of A_1 symmetry at about 45 cm^{-1} at room temperature and a strong line at 50 cm^{-1} that he identified as a B_1 mode, but gave no other details of the spectrum. Higher-wave-number lines have been associated with molybdate-group vibrations.[4] In this paper, observations of 90°-scattered Raman spectra extending to 3000 cm^{-1} for several crystal orientations and covering the temperature range from room temperature to above T_c are described. An analysis of these data is given in which the spectra for wave numbers less than 1000 cm^{-1} are classified.

GMO has a relatively complex structure with 68 atoms per crystallographic cell in its orthorhombic (C_{2v}) phase below T_c (~160 °C) and 34 atoms per cell in its tetragonal (D_{2d}) phase above T_c. The tetragonal cell is rotated 45° about the polar axis relative to the orthorhombic cell and has half the volume. (Crystallographic details have been given by Keve *et al.*[5] and Jeitschko.[6]) The dynamic instability that drives the transition into the ferroelectric phase on cooling has been predicted[7,8] and shown[9,10] to be the softening of two degenerate zone-boundary (M-point) phonons that, because of the cell doubling, become zone-center phonons (and hence, optically active) below T_c.

II. EXPERIMENTAL DETAILS

Measurements were made on samples cut from a boule purchased from the Isomet Corporation. Samples were cut and polished into approximately 2-mm-edge cubes. The c faces were normal to the polar c axis in all cases. The other faces were cut with both {110} and {100} orientations to obtain measurements on samples with edges parallel to crystal axes in at least one phase or the other; because of the 45° rotation of the cell about the polar axis on heating above T_c, this cannot be achieved with one sample for both phases without rotating the crystal. The faces were then polished with a minimum abrasive grit of 0.05 μm.

Crystals were poled by cooling through T_c with 7500-V/cm electric fields applied through semitransparent gold electrodes in the polar direction (the coercive field is ~5 kV/cm) and simultaneously were viewed through a polarizing microscope. In some cases, domain walls remained near the corners of the crystal. These areas were avoided in the experiments by directing the laser beam through the center of the crystal.

Spectra were obtained with a Spex model No. 1401 Raman spectrometer equipped with a Coherent Radiation Laboratory argon-ion laser with about 1 W of output in either the 4880- or 5145-Å lines. The data reported here are mostly for

4880-Å excitation; the 5145-Å line was also used in some cases. The scattered light was focused on the spectrometer slit with a 50 mm $f/0.95$ lens. A quarter-wave plate was used to rotate the polarization of the incident beam by 90° when desired.

The crystal was cemented to a capillary tube and mounted in a glass tube in which hot air could be circulated. (A few expanded-scale spectra, described later, were measured from a crystal mounted on a heated stage in an evacuated chamber.) A thermocouple situated in the air stream close to the sample monitored the temperature.

For all spectra, the spectrometer slit widths were less than 100 μm assuring a resolution of less than 2 cm^{-1}. Examination of the data indicates a precision in wave-number determination with a mean deviation less than ± 2 cm^{-1}. (The expanded scale that was required in some cases is described later in the text.)

III. ANALYSIS

Throughout this paper, the orientation and polarization of the incident and scattered beams relative to the crystal axes are described by a notation now in frequent use. The four quantities required to describe an experimental configuration are arranged in sequence with the two central ones enclosed in parentheses: $A(BC)D$, where A is the incident-beam direction, B is the incident-beam polarization, C is the scattered-beam polarization, and D is the scattered-beam direction. Each quantity is represented by a coordinate x, y, or z or pair of coordinates xy, yz, xz for propagation along a crystallographic cell-face diagonal. Bars over coordinates indicate a negative direction. Commas are sometimes inserted between B and C for clarity.

The symmetries of the Raman-active phonons that can participate in the scattering process for a given experimental configuration can be determined by inspection of the matrix representations of the Raman tensors for the appropriate crystallographic point groups as tabulated by Loudon.[11] The representations for the two phases of GMO studied here, $D_{2d}(T > T_c)$ and $C_{2v}(T < T_c)$ are shown in Table I.

TABLE I. Raman tensors.

Crystal class	Raman tensors				
$C_{2v}(mm2)$	$\begin{pmatrix} a & 0 & 0 \\ 0 & b & 0 \\ 0 & 0 & c \end{pmatrix}$	$\begin{pmatrix} 0 & d & 0 \\ d & 0 & 0 \\ 0 & 0 & 0 \end{pmatrix}$	$\begin{pmatrix} 0 & 0 & e \\ 0 & 0 & 0 \\ e & 0 & 0 \end{pmatrix}$	$\begin{pmatrix} 0 & 0 & 0 \\ 0 & 0 & f \\ 0 & f & 0 \end{pmatrix}$	
	$A_1(z)$	A_2	$B_1(x)$	$B_2(y)$	
$D_{2d}(\bar{4}2m)$	$\begin{pmatrix} a & 0 & 0 \\ 0 & a & 0 \\ 0 & 0 & b \end{pmatrix}$	$\begin{pmatrix} c & 0 & 0 \\ 0 & -c & 0 \\ 0 & 0 & 0 \end{pmatrix}$	$\begin{pmatrix} 0 & d & 0 \\ d & 0 & 0 \\ 0 & 0 & 0 \end{pmatrix}$	$\begin{pmatrix} 0 & 0 & e \\ 0 & 0 & 0 \\ e & 0 & 0 \end{pmatrix}$	$\begin{pmatrix} 0 & 0 & 0 \\ 0 & 0 & e \\ 0 & e & 0 \end{pmatrix}$
	A_1	B_1	$B_2(z)$	$E(y)$	$E(x)$

TABLE II. Correlation table for D_{2d} and C_{2v} point groups.

D_{2d}	C_{2v}
A_1	A_1
A_2	A_2
B_1	A_2
B_2	A_1
E	$B_1 + B_2$

Further selection can be made by carrying out scattering-efficiency calculations which include, in addition to the beam polarizations, their propagation directions and the polarizations of the interacting phonons. Scattering-efficiency calculations were made using Loudon's theory[11] for piezoelectric uniaxial crystals. GMO is biaxial in the C_{2v} phase but at the time of these calculations, no theory for the biaxial case was available. (The theory for this case has appeared recently.[12]) However, in GMO the deviation from uniaxiality is small,[2] suggesting that the uniaxial theory as given by Loudon could have at least approximate validity below T_c.

Calculations of the scattering intensity for both phases were made for all of the combinations of incident-beam direction and polarization studied. For each case, separate calculations were made for the scattered-beam polarization either parallel or perpendicular to the scattering plane. Three different phonons were considered for each scattered-beam polarization: longitudinal, transverse in the scattering plane, and transverse perpendicular to the scattering plane. Long-range electrostatic forces were assumed to predominate over the anisotropy of short-range interatomic forces so that the electric field associated with the polar vibrations would be approximately parallel to the longitudinal phonon.

It is also possible, in some cases, to make symmetry assignments by comparison with the normal modes of free molecules. Comparisons of the infrared spectra of molybdates and other similar compounds, such as tungstates, reveal marked similarities in the 200–1000-cm^{-1} range. Many of these lines are also observed in the Raman spectra. Consequently, an analysis based on line splitting of the normal modes of free XY_4 molecules was tested and found to provide a convenient and straightforward means for identifying the higher-frequency lines in the spectra, i.e., in the 200–1000-cm^{-1} range.

The Raman lines group naturally, in any case, into a low- and high-frequency region so the ex-

perimental results, described below, are classified correspondingly.

IV. EXPERIMENTAL RESULTS

A. The 0-200-cm^{-1} Range

The correlation table connecting the allowed symmetries for the low- and high-temperature phases is shown in Table II. The results of the scattering-efficiency and symmetry analyses applied to the spectra taken of both phases in twelve different experimental configurations are shown in Tables III and IV. Typical examples of spectra for these symmetries are shown in Figs. 1 and 2. "Forbidden" lines appear quite often with significant intensity. This could arise in part from a combination of imperfect crystal alignment, highly convergent optics, and crystal imperfections, and some mode mixing from optical rotation could have occurred since $n_e - n_o \sim 6 \times 10^{-3}$ for GMO. Also, phonons propagating along directions other than the principal axes can have mixed symmetry.[13] The analysis in Table III is based on the highest-intensity lines, the predictions of the correlation table (Table II), and the scattering-efficiency analysis.

A special set of expanded-scale measurements was required to obtain the splitting of the high-temperature E modes into the B_1 and B_2 modes at low temperature; these are shown in Fig. 3.

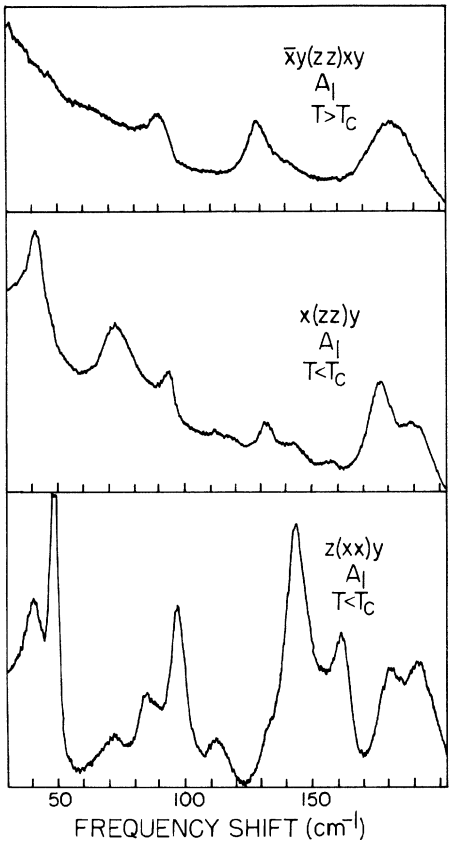

FIG. 1. A_1 Raman spectra, 0–200 cm^{-1}, at high temperature and room temperature. Note the disappearance of the 43-cm^{-1} "Fleury" line at $T > T_c$.

TABLE III. Observed Raman lines, 0–200 cm^{-1}.

D_{2d} Symmetry	D_{2d} Wave number (cm^{-1})	C_{2v} Wave number (cm^{-1})	C_{2v} Symmetry
		43	A_1
A_1	180	180	A_1
B_1	50[a]	50	A_2
A_2	Raman inactive	75[b]	A_2
B_1	115	115	A_2
B_2	98	98	A_1
B_2	144	144	A_1
B_2	160	160	A_1
E	90	90	B_1
		98	B_2
E	130	135	B_1
		138	B_2
E	190	192	B_1
		196	B_2
		63	B_1, B_2
		110	B_1, B_2
		119	B_1, B_2

[a]The 50-cm^{-1} line appears strongly in all orientations with x or y (or both) polarization. It was significantly stronger, however, in the orientations indicated above.

[b]Since the 75-cm^{-1} line has comparable intensity in both A_1 and A_2 spectra it could also be classified as an A_1 mode in C_{2v} that becomes a zone-boundary mode in D_{2d}.

The three lines listed at the bottom of Table III appear with significant intensity at low temperature as B_1, B_2, or both, but are absent at high temperature, suggesting that they are zone-boundary modes in the high-temperature phase, as discussed below.

B. The 200-1000-cm^{-1} Range

The second group of lines, appearing above 200 cm^{-1}, is clearly distinguishable from the lower-frequency lines, since their intensities are about an order of magnitude greater, their bandwidths are about a factor of 4 narrower, and the temperature dependence of both intensity and bandwidth is weak or absent.

The point symmetry of the XY_4 molecule is T_d; the correlation table connecting this group with the low- and high-temperature GMO point groups is given in Table V. The free $MoO_4^{=}$-ion frequencies and symmetries[14] are listed in the first column of Table VI.

All of the lines observed in this range are shown in Table VI. Again, a special set of expanded-

TABLE IV. Experimental configurations and associated phonon polarizations determined from scattering-efficiency calculations (T = transverse, L = longitudinal).

A_1(ir inactive)	B_1(ir inactive)	D_{2d} phase B_2	E
$x(zz)y$ $\bar{x}y(zz)xy$	$z(xx)y$ $xy(x\bar{y},xy)z$ $\bar{x}y(xy,\bar{x}y)xy$	$xy(x\bar{y},x\bar{y})z - L_{xyz}$ $z(\bar{x}y,\bar{x}y)xy - L_{xyz}, T_{xyz}$	$\bar{x}y(xy,z)xy - L_x, L_y$ $\bar{x}y(z,\bar{x}y)xy - L_{xyz}, T_{xyz}$ $x(zx)y - L_{xy}, T_{xy}$ $z(xz)y - L_{xz}, T_{xz}$
A_1	A_2(ir inactive)	C_{2v} phase B_1	B_2
$x(zz)y - T_z$ $\bar{x}y(zz)xy - T_z$ $x(yy)z - L_{xz}, T_{xz}$ $z(xx)y - L_{yz}, T_{yz}$	$x(yx)z$ $x(yx)y$ $z(xy,xy)\bar{x}$	$x(zx)y - L_{xy}, T_{xy}$ $z(xy)y - T_x$ $\bar{x}y(z,\bar{x}y)xy - L_x, T_y$ $z(xy,z)\bar{x}y - L_{xyz}, T_{xyz}, T_{xy}$	$x(yz)y - L_{xy}, T_{xy}$ $\bar{x}y(z,xy)xy - L_x, T_y$ $z(xy,z)\bar{x}y - L_{xyz}, T_{xyz}, T_{xy}$

scale measurements was required to observe the splittings of the E modes. Typical spectra are shown in Figs. 4–8. Three lines in Table VI deviate from the behavior predicted by the symmetry analysis. The 817-cm^{-1} line in D_{2d} does not have a corresponding doublet in C_{2v}, suggesting either anomalous behavior or insufficient instrumental resolution (of the order of ±1 cm^{-1} in these measurements, even with the expanded scale). The B_1 291- and 299-cm^{-1} lines are, if present, masked in B_2 spectra by the stronger 288- and 307-cm^{-1} lines but are labeled $B_{1,2}$ in Table VI, since no corresponding D_{2d} mode was observed. Hence these also could be identified as zone-boundary modes in D_{2d}.

V. DISCUSSION OF RESULTS

Differences in the low- and high-temperature spectra are expected on two counts. First, lines

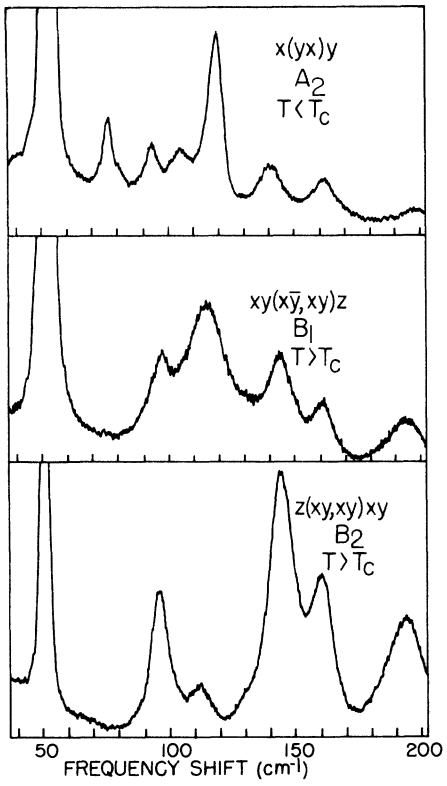

FIG. 2. High-temperature B_1 and B_2 Raman spectra and room-temperature A_2 spectrum, 0–200 cm^{-1}.

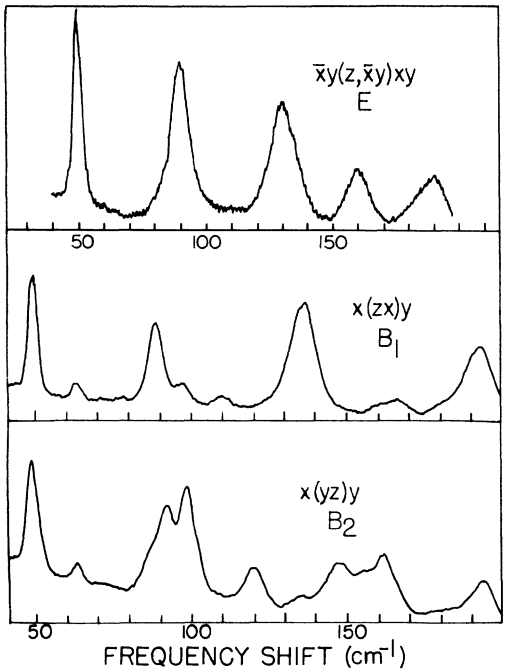

FIG. 3. High-temperature E Raman spectrum and expanded scale B_1 and B_2 room-temperature spectra, 0–200 cm^{-1}.

TABLE V. Correlation table for T_d, D_{2d}, and C_{2v} point groups.

T_d	D_{2d}	C_{2v}
A_1	A_1	A_1
A_2	B_1	A_2
E	A_1+B_1	A_1+A_2
F_1	A_2+E	$A_2+B_1+B_2$
F_2	B_2+E	$A_1+B_1+B_2$

in the C_{2v} phase will coalesce or disappear in the D_{2d} phase simply as a consequence of the change to higher symmetry and the concomitant selection rules. Second, the crystallographic cell of GMO is known to double in volume on cooling from D_{2d} to C_{2v}. Consequently, zone-boundary modes in D_{2d} can be Raman active in C_{2v}. If the dispersion curves are not flat, such zone-boundary modes will appear as lines in C_{2v} that have no corresponding lines in D_{2d}. We have observed six lines of this type: 43, 63, 110, 119, 291, and 299 cm^{-1}.

There are many more modes, of course, but their frequencies may be too close to the zone-center frequency (flat dispersion curve) to be distinguished.

The 43-cm^{-1} mode, as first reported by Fleury,[3] decreases in intensity and shifts to lower frequency on heating toward T_c. It appears to be associated with one or both of the zone-boundary modes in D_{2d} whose instability at T_c cause the transition.[9,10] The 50-cm^{-1} mode, also observed by Fleury, has been reported to be a B_1 mode in C_{2v} that becomes an E mode in D_{2d}.[3,9,10] We find the highest intensity for this line in A_2 orientations in C_{2v} and B_1 orientations in D_{2d}: hence the identification in Table III. However, it appears as a strong line in all scattering configurations except those with both incident and scattered radiation polarized along the c axis (zz). Probably, there are phonons of this frequency with each of the possible symmetries, but restricted to the a-b plane. Nonetheless, our data indicate the highest scattering efficiency for the A_2 phonon in C_{2v}. This is not necessarily inconsistent with earlier work. Fleury[3] did not report results on an A_2 configuration

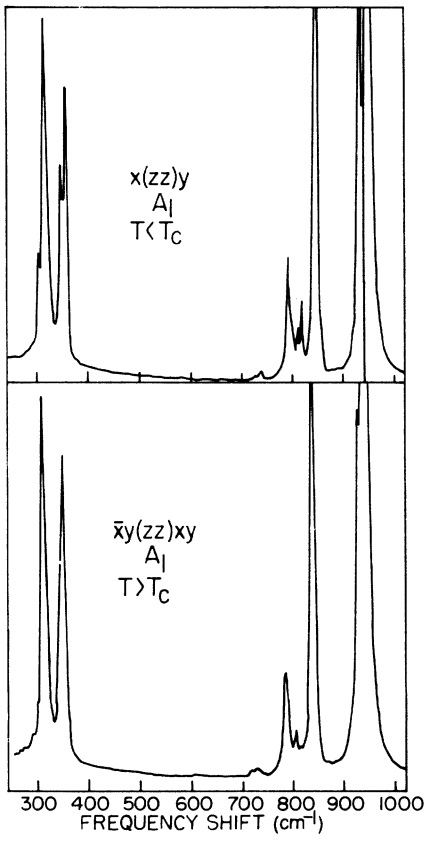

FIG. 4. Raman spectra, 200–1000 cm^{-1}, of transverse A_1 modes at high temperature and room temperature.

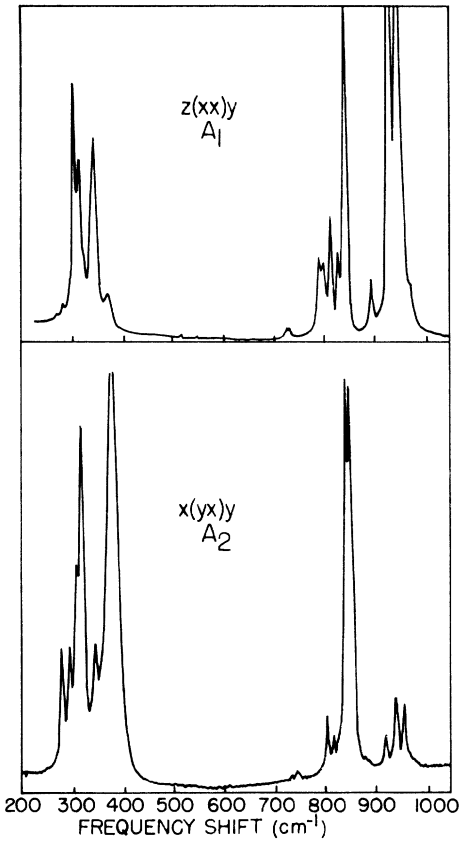

FIG. 5. A_1 and A_2 Raman spectra, 200–1000 cm^{-1}, at room temperature.

TABLE VI. Observed Raman lines and their identification, 200–1000 cm^{-1}.

T_d		D_{2d}		C_{2v}	
Wave number (cm^{-1})	Symmetry	Wave number (cm^{-1})	Symmetry	Wave number (cm^{-1})	Symmetry
$\nu_1 = 894$	A_1	800	A_1	800	A_1
		absent	absent	827	A_1
		855	A_1	855	A_1
		940	A_1	940	A_1
		960	A_1	960	A_1
$\nu_2 = 381$	E	300	B_1	300	A_2
		315	B_1	315	A_2
		350	A_1	350	A_1
		360	A_1	360	A_1
		385	B_1	385	A_2
$\nu_3 = 833$	F_2	731	E	727	B_1
				737	B_2
		742	E	748	B_1
				750	B_2
		796	B_2	801	A_1
		807	B_2	813	A_1
		817	E	821	$B_{1,2}$
		827	E	828	B_1
				830	B_2
		835	E	837	B_1
				840	B_2
		844	E	847	B_1
				848	B_2
		847	B_2	847	A_1
		879	E	882	B_1
				883	B_2
		915	E	915	B_1
				921	B_2
		930	E	930	B_1
		941	B_2	942	A_1
		954	B_2	958	A_1
		965	E	965	B_1
$\nu_4 = 318$	F_2	279	E	284	B_1
				288	B_2
		281	B_2	282	A_1
		298	B_2	296	A_1
		306	E	306	B_1
				307	B_2
		308	B_2[a]	308	A_1
		320	B_2	323	A_1
		325	E	327	B_1
				328	B_2
		330	B_2	330	A_1
		341	E	342	B_2
				345	B_1
		361	B_2	362	A_1
		380	B_2	384	A_1
		404	E	407	B_1
				417	B_2
				291	$B_{1,2}$
				299	$B_{1,2}$

[a]The 308-cm^{-1} line is masked by the intense doublet at 320 and 330 cm^{-1} (see Fig. 8).

and since A_2 modes are not ir active, it also would not have been observed by Petzelt and Dvorak.[10]

Attempts to delineate the temperature dependences of the Raman line intensities were not successful. The structure changes continuously in C_{2v} on heating toward T_c,[6] so it was not possible

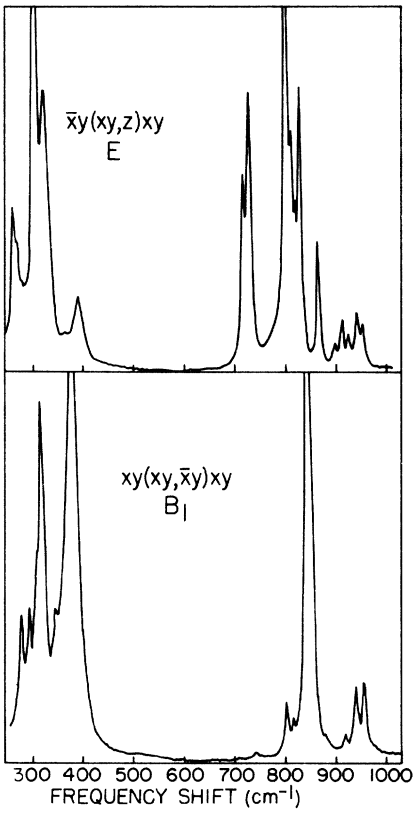

FIG. 6. E and B_1 Raman spectra, 200–1000 cm^{-1}, at high temperature.

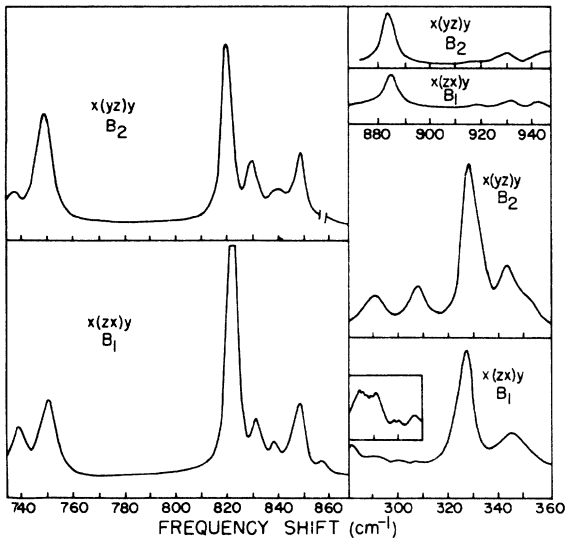

FIG. 7. B_1 and B_2 expanded-scale Raman spectra, 200–1000 cm^{-1}, at room temperature. Inset on B_1 260–360-cm^{-1} spectrum has vertical scale expanded × 10 to show weak lines in 280–300-cm^{-1} range.

in these studies to separate the temperature dependence arising from structural changes from the simultaneous changes in phonon population. Consequently, we have considered all of the observed lines to be first order; the possibility that some are second order (or higher) certainly cannot be ignored.

Great care was taken in this work to ensure that the sample was poled. To determine the importance of such precautions, a few measurements were made on unpoled samples. Differences between poled and unpoled spectra were observed only in B_1 and B_2 orientations. This is readily explained by the crystallographic orientation of the domains. Adjacent domains are related by a $\bar{4}$-point symmetry operation which interchanges the a and b axes (i.e., $a \rightarrow -b$ and $b \rightarrow a$). Thus the domain symmetry alternates between B_1 and B_2 for incident and scattered polarizations in the a-b plane, and thus a mixing of B_1 and B_2 modes should be expected in unpoled samples. Further evidence of this behavior is observed by applying electric fields parallel to the polar axis or a shear stress in the a-b plane to single-domain samples. The field or stress switches the crystal and corresponding changes in the Raman spectrum between B_1 and B_2 are observed.

The work described herein is the first step to-

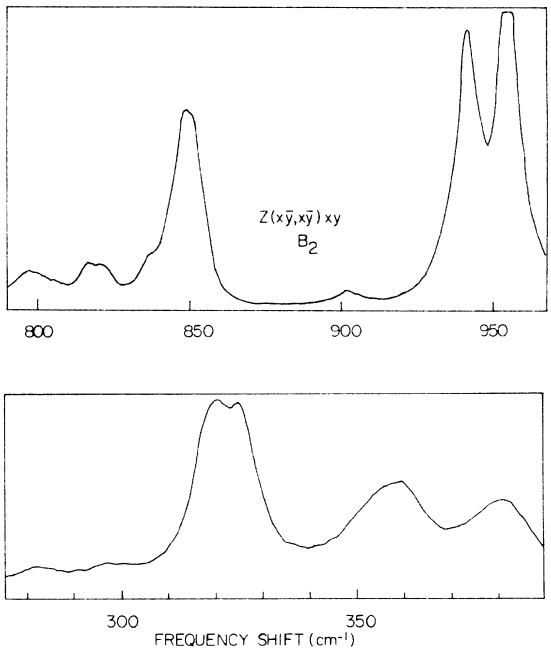

FIG. 8. B_2 expanded scale Raman spectrum, 200–1000 cm^{-1}, at high temperature. (The 308-cm^{-1} line is masked by the intense doublet at 320 and 330 cm^{-1}; see Table VI.)

ward obtaining an understanding of some of the lattice-dynamical properties of rare-earth molybdates from Raman-scattering studies. Now that the spectrum has been classified, the dependence of individual lines on temperature, pressure, or other parameters can be studied in detail.

ACKNOWLEDGMENTS

The authors are grateful to M. Hass and R. D. Kirby for their advice and guidance and to DuPont Chemical Corporation and Isomet Corporation for providing some of the crystals studied.

---

*Research sponsored by the Air Force Office of Scientific Research, Office of Aerospace Research, USAF under Grant No. AFOSR-70-1926. The United States Government is authorized to reproduce and distribute reprints for Governmental purposes notwithstanding any copyright notation hereon.

†A portion of this work is based on a dissertation submitted by B. J. Holden in partial fulfillment of the requirements for the Ph.D. degree.

‡Present address: Naval Weapons Center, China Lake, Calif.

[1]L. E. Cross, A. Fouskova, and S. E. Cummins, Phys. Rev. Lett. **21,** 812 (1968).

[2]S. E. Cummins, Ferroelectrics **1,** 11 (1970).

[3]P. A. Fleury, Solid State Commun. **8,** 601 (1970).

[4]I. W. Shepherd and J. R. Barkley, Solid State Commun. **10,** 123 (1972).

[5]E. T. Keve, S. C. Abrahams, and J. L. Bernstein, J. Chem. Phys. **54,** 3185 (1971).

[6]W. Jeitschko, Acta. Cryst. B **28,** 60 (1972).

[7]E. Pytte, Solid State Commun. **8,** 2101 (1970).

[8]V. Dvorak, Phys. Status Solidi B **45,** 147 (1971).

[9]B. Dorner, J. D. Axe, and G. Shirane, Phys. Rev. Lett. **26,** 519 (1971); Phys. Rev. B **6,** 1950 (1972).

[10]J. Petzelt and V. Dvorak, Phys. Status Solidi B **46,** 413 (1971); J. Petzelt, Solid State Commun. **9,** 1485 (1971).

[11]R. Loudon, Adv. Phys. **13,** 423 (1964).

[12]A. S. Barker, Jr. and R. Loudon, Rev. Mod. Phys. **44,** 18 (1972).

[13]E. Anda, Solid State Commun. **9,** 1545 (1971).

[14]R. H. Busey and O. L. Keller, Jr., J. Chem. Phys. **41,** 215 (1964).